Self-assembled boron-doped graphene nanoribbons: electronic structure and Raman fingerprints

Boris V. Senkovskiy,[*,†] Dmitry Yu. Usachov,[‡] Alexander V. Fedorov,[†,‡,¶] Tomas Marangoni,[§] Danny Haberer,[§] Cesare Tresca,[‖] Gianni Profeta,[‖] Vasile Caciuc,[#] Shigeru Tsukamoto,[#] Nicolae Atodiresei,[#] Niels Ehlen,[†] Chaoyu Chen,[@] Jose Avila,[@] Maria C. Asensio,[@] Andrei Varykhalov,[△] Alexei Nefedov,[▽] Christof Wöll,[▽] Timur K. Kim,[††] Moritz Hoesch,[††] Felix R. Fischer,[§] and Alexander Grüneis[*,†]

II. Physikalisches Institut, Universität zu Köln, Zülpicher Strasse 77, 50937 Köln, Germany, St. Petersburg State University, 7/9 Universitetskaya nab., St. Petersburg, 199034, Russia, IFW Dresden, P.O. Box 270116, Dresden D-01171, Germany, Department of Chemistry, University of California at Berkeley, Tan Hall 680, Berkeley, CA 94720, USA, Department of Physical and Chemical Sciences and SPIN-CNR, University of L'Aquila , Via Vetoio 10, I-67100 Coppito, Italy, Institut des Nanosciences de Paris, Sorbonne Universités-UPMC univ Paris 6 and CNRS-UMR 7588, 4 place Jussieu, F-75252 Paris, France, Peter Grünberg Institut (PGI-1) and Institute for Advanced Simulation (IAS-1), Forschungszentrum Jülich and JARA, D-52425 Jülich, Germany, ANTARES Beamline, Synchrotron SOLEIL & Universite Paris-Saclay, L' Orme des Merisiers, Saint Aubin-BP 48, 91192 Gif sur Yvette Cedex, France, Helmholtz-Zentrum Berlin für Materialien und Energie, Berlin, Germany, Institut für Funktionelle Grenzflächen (IFG), Karlsruher Institut für Technologie (KIT), Hermann-von-Helmholtz-Platz 1, 76344 Eggenstein-Leopoldshafen, Germany, and Diamond Light Source, Harwell Campus, Didcot, OX11 0DE, United Kingdom

E-mail: senkovskiy@ph2.uni-koeln.de; grueneis@ph2.uni-koeln.de

Abstract

We show that strong chemical interaction between boron doped graphene nanoribbons with $N = 7$ atoms width (B-7AGNRs) and an Au substrate leads to periodic out-of-plane corrugation and electron doping of B-7AGNRs. Using angle-resolved photoemission spectroscopy (ARPES), we find that the dopant-derived bands hybridize with substrate electronic states and spread in energy. The interaction with the substrate leaves the bands with pure carbon character unperturbed. This results in an identical effectives mass of $\sim 0.2\ m_0$ compared to pristine 7AGNRs. The presence of boron atoms further manifests in the vibrational properties. We probe the phonons of B-7AGNRs *in situ* by Raman spectroscopy. We reveal the existence of characteristic splittings and red-shifts of Raman modes due to the presence of C-B bonds. The strongly hybridized electronic structure of the B-7AGNR - Au contact can be useful for carbon based nanoelectronics. The Raman fingerprint allows easy identification in device geometries.

Introduction

Doping a semiconductor by foreign atoms of a different valency is a means to shift the chemical potential and to engineer the carrier concentration providing the basis for modern

*To whom correspondence should be addressed

†II. Physikalisches Institut, Universität zu Köln, Zülpicher Strasse 77, 50937 Köln, Germany

‡St. Petersburg State University, 7/9 Universitetskaya nab., St. Petersburg, 199034, Russia

¶IFW Dresden, P.O. Box 270116, Dresden D-01171, Germany

§Department of Chemistry, University of California at Berkeley, Tan Hall 680, Berkeley, CA 94720, USA

‖Department of Physical and Chemical Sciences and SPIN-CNR, University of L'Aquila , Via Vetoio 10, I-67100 Coppito, Italy

⊥Institut des Nanosciences de Paris, Sorbonne Universités-UPMC univ Paris 6 and CNRS-UMR 7588, 4 place Jussieu, F-75252 Paris, France

#Peter Grünberg Institut (PGI-1) and Institute for Advanced Simulation (IAS-1), Forschungszentrum Jülich and JARA, D-52425 Jülich, Germany

@ANTARES Beamline, Synchrotron SOLEIL & Universite Paris-Saclay, L' Orme des Merisiers, Saint Aubin-BP 48, 91192 Gif sur Yvette Cedex, France

△Helmholtz-Zentrum Berlin für Materialien und Energie, Berlin, Germany

▽Institut für Funktionelle Grenzflächen (IFG), Karlsruher Institut für Technologie (KIT), Hermann-von-Helmholtz-Platz 1, 76344 Eggenstein-Leopoldshafen, Germany

††Diamond Light Source, Harwell Campus, Didcot, OX11 0DE, United Kingdom

electronic devices. Semiconducting graphene nanoribbons (GNRs) have a great potential for nanoelectronics and optics, since their structure can be engineered with atomic precision by bottom-up synthesis from molecular precursors and their electronic band structure can be tuned in a wide range.[?,?,?,?,?,?,?] This fabrication approach allows for the doping of GNRs by heteroatoms and functional groups in an easy way by precursor choice.[?,?,?,?,?] Recently, the incorporation of boron atoms, acting as p-type dopants, into the lattice of armchair graphene nanoribbons of N=7 carbon atoms width (7AGNRs) has been demonstrated.[?,?] The pairs of boron atoms in the synthesized B-7AGNRs are periodically embedded in the carbon backbone at defined positions, forming a superstructure along the ribbon axis. The situation of atomically precise doping is quite unique. For example, the sublattice specific incorporation of boron in epitaxial graphene has been demonstrated,[?] but it by far lacks ~~the~~ perfection that can be achieved by bottom-up nanotechnology. Indeed, if the dopant atoms occupy random positions of the graphene lattice, the perturbations in the periodic potential contribute to momentum scattering of charge carriers limiting the electron mobility.[?] However, if heteroatoms are periodically incorporated in the crystal, translational symmetry and hence momentum conservation is preserved.[?,?] This clearly should improve transport characteristics of B-doped GNRs, which are very interesting for technological applications as gas sensors, solar cell components or electrocatalysts.[?,?,?] Heterojunctions of pristine and B-doped 7AGNRs attract attention in the context of electronic transport.[?] It has also been predicted theoretically, that B-doped and pristine 7AGNR segments fused together exhibit antiferromagnetic coupling.[?] Therefore, it is mandatory for the field to unambiguously determine the energy band structure of B-doped GNRs.

Intuitively, one expects that the incorporation of boron atoms (having one electron less than the carbon host) result in hole doping. The periodicity of boron is expected to lead to the formation of two bands above and below the Fermi level with significant boron contribution to the density of states and a weak dispersion, which is due to the low wave function overlap of boron orbitals. Such bands forming valence and conductions bands of B-7AGNRs

were found in *ab initio* calculations.[? ?] However, there is no clear observation of these bands by scanning tunneling spectroscopy (STS). Indeed, the STS measurements of B-doped 7AGNRs on Au(111) surprisingly reveal the same value of quasiparticle band gap as for the pristine system – 2.4 eV.[?] Theory based on GW approximation (which include screening of the electron-electron interaction by the metal substrate) predicts the energy separation between the dopant-derived bands in B-7AGNRs of only 0.8 eV and the band gap in 7AGNRs of 2.1 eV.[?] This discrepancy may be due to the fact that in realistic systems, B-7AGNR electronic band structure can be affected by the substrate, which has not been explored yet.

Moreover, an easy and quick fingerprinting method is needed by the nanoribbon community to identify B-7AGNRs with good spatial resolution for future applications in device configurations. Raman spectroscopy is such a technique and has been applied to characterize GNRs of numerous types.[? ? ? ? ? ? ? ? ?] However, the Raman spectrum of B-7AGNRs is still elusive. The present work addresses these issues by a detailed experimental investigation using angle-resolved photoemission spectroscopy (ARPES) and *in situ* ultra-high vacuum (UHV) Raman spectroscopy to unravel the changes in the electronic structure and vibrational properties of 7AGNRs induced by the periodically incorporated B atoms. Our studies are supported by X-ray photoelectron and absorption spectroscopies as well as by density functional theory (DFT) calculations of the electronic and vibrational properties.

Results and Discussion

Stoichiometry and corrugation Aligned B-7AGNRs were synthesized on vicinal Au(788) crystal with narrow (111) terraces using a similar recipe previously applied for synthesis on Au(111)[? ?] (see Methods). The alignment is needed for ARPES and polarized Raman measurements, discussed in the following sections. The chemical state, composition and the structure of synthesized B-7AGNRs were probed by X-ray photoelectron spectroscopy (XPS) and near-edge X-ray absorption fine structure (NEXAFS) spectroscopy studies. Figure 1(a)

illustrates different chemical environments of carbon atoms present in B-7AGNRs. There are C atoms surrounded by three other C atoms (denoted as C_1) or having only two C neighbours and either H or B as a third neighbour (C_2 and C_3, respectively). Figure 1(b) depicts XPS spectra of B-7AGNRs in the region of C 1s and B 1s core-levels. The C_1 component's energy is 284.05 eV, which is $\sim$ 0.15 eV smaller than for pristine 7AGNRs.[?] The C_2 component appears at 283.90 eV and the C_3 component at 283.00 eV. Similar to C_3 low energy component was also observed in the B-doped epitaxial graphene.[?] We obtain an intact B/C = 1/20 ratio that is expected on the basis of the structure. The B 1s peak consists of one component at 186.8 eV. When B-doped GNRs are exposed to air, they rapidly oxidize and the B 1s peak splits into two components (see Fig. S1 in Supplementary Information). The high chemical reactivity of the boron sites is consistent with previous observations in boron doped graphene sensors[?] and is highly relevant for the substrate interaction effects as we will show later.

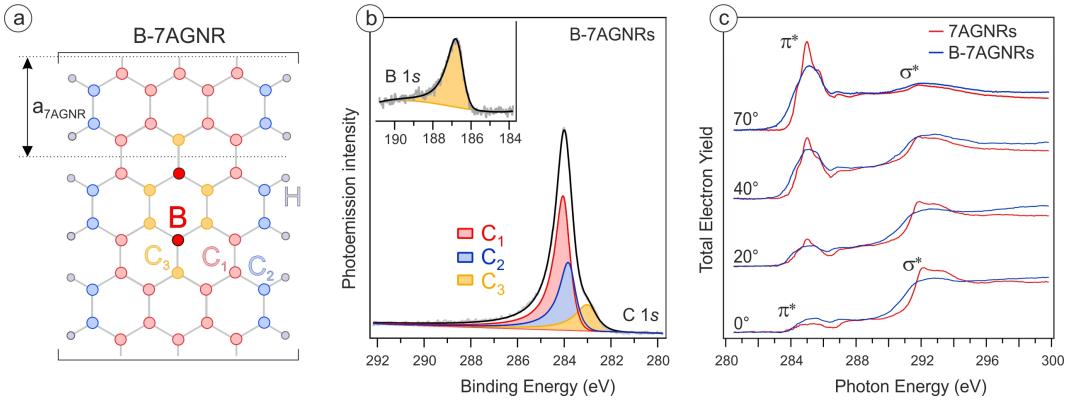

Figure 1: (a) Unit cell of hydrogen-terminated B-7AGNRs containing C atoms surrounded by three other C atoms (C_1), C atoms next to an H atom (C_2) and next to a B atom (C_3). The lattice parameter of pristine 7AGNRs is marked as a_{7AGNRs}. (b) XPS spectra of the C 1s and the B 1s core levels of B-7AGNRs/Au(788). The C 1s spectrum consists of three components (C_1-C_3) which correspond to the different chemical environment of C atoms. (c) Comparison of the C K-edge NEXAFS spectra of pristine and B-doped 7AGNRs on Au(788) at different angles between the light polarization and the sample surface.

Let us now look at the C K-edge NEXAFS spectra which relate to the transitions from the C 1s core levels to unoccupied π^* and σ^* states. According to the selection rules for X-ray

absorption, the π^* (σ^*) resonance should be suppressed (enhanced) when the incident light is polarized along the flat sheet of sp^2 bonded carbon and enhanced (suppressed) when the light has out-of-plane polarization. Comparing pristine and B-doped 7AGNRs in Figure 1 (b), one can find that for normal incidence of linearly polarized radiation (0°) the π^* resonance has a higher intensity and the σ^* resonance has a lower intensity in B-7AGNRs. Based on the angular dependence of the matrix element, this behavior suggests that, unlike to the pristine system, B-7AGNRs are not lying flat on the Au substrate but are corrugated. The corrugation has never been directly measured. However, a frequency shift was observed[?] in atomic force microscopy experiments when the tip was placed upon a borylated segment. This frequency shift, together with calculations hinted at the corrugation of B-7AGNRs on Au. Interestingly, in B-7AGNRs a new contribution in π^* resonance is rising below 284 eV with increasing angle and becoming most pronounced for grazing incidence (70°). This low energy shoulder is associated with the C_3 atoms having lowest binding energy and its disappearance at 0° suggests that the out-of-plane structural distortion is mostly related to the C_1 and C_2 atoms. This may be if B atoms are pulling the nearest neighbour carbons towards the Au surface forcing the rest nanoribbon structure to buckle. The interaction of B sites with the substrate should affect the electronic band structure of B-7AGNRs.

Electronic band structure

The electronic states confined in the quasi-one-dimensional (quasi-1D) GNRs have continuous dispersion along the momentum parallel to the ribbon axis ($k_\parallel$) while there are only a discrete set of allowed values along the transverse momentum ($k_\perp$) direction. We have recently demonstrated that the photoemission intensity for a given electronic energy band in GNRs is a function of 2D momentum (i.e. $k_\parallel$ and $k_\perp$) and the binding energy.[?] By scanning $k_\perp$ we seek to maximize photoemision from specific bands of nanoribbon electronic states.[?] Thus, ARPES mapping of the full two-dimensional (2D) momentum space is needed to visualize and unambiguously determine all valence bands of 1D nanoribbons. In the following we apply this approach to reveal the electronic energy band structure of B-7AGNRs.

Figure 2 (a) shows an ARPES scan of B-7AGNRs/Au(788) accumulated along $k_{\|}$ at constant $k_{\perp} = 0$ Å^{-1}. The scan path relative to the 2D graphene BZ is shown as an inset in the upper right corner of the figure. This ARPES scan reveals two nanoribbon-derived electronic states: a flat band at 1.71 eV (marked by an orange arrow in Fig. 2 (a)) and a faint parabolic band (marked by a red arrow). Here and in the following we count the first and the second valence bands measuring their energy from the Fermi level and label them as VB and VB-1, respectively. Figure 2 (b) shows the corresponding DFT calculations carried out for freestanding B-7AGNRs (see Methods). Here the energy is taken as zero (Fermi level) in the center of the band gap. The thickness of the bands in Figure 2 (b) reflects the photoemission intensity at $k_{\perp} = 0$ Å^{-1}. These calculations are similar to what has been done by us for 7-AGNRs.[?] From the calculations we obtain that the bands of B-7AGNRs acquiring sufficiently large photoemission intensity are centered at approximately the edge of graphene BZ ($k_{\|} = 1.47$ Å^{-1}). Assuming no bond-length change, the unit cell of B-7AGNRs is equal to 3 times the size of the unit cell of 7AGNRs (Fig. 1 (a)). Thus the measured bands are in the fourth 1D BZ of B-7AGNRs. Particularly, as seen in Figure 2(b), two weakly dispersing (flat) bands should be observed at $k_{\perp} = 0$ Å^{-1} according to the calculations. The highest one (VB) is marked by an orange arrow and the low-energy flat band by a blue arrow. Importantly, the second valence band (VB-1) with parabolic dispersion shown by the red arrow is predicted to have much weaker ARPES intensity in this experimental geometry. Comparing the experiment to calculations, we find agreement for the energetically lower flat band and the low-intensity parabolic band. ARPES does not reveal the theoretically predicted VB close to the Fermi energy, marked by a blue arrow in Figure 2 (b). Previous STS measurements of B-7AGNRs on Au(111) also did not identify this band.[? ?] The fact that this flat band is absent in the experiments is a hint towards hybridization of the dopant-derived bands with the electronic states of Au substrate. We will treat this effect in detail in the following section.

Let us now perform a similar analysis as the one displayed in Figures 2 (a) and (b) for a

different value of $k_\perp$ in order to vary the most intense band. Figure 2 (c) depicts an ARPES scan at $k_\perp = -0.4$ Å^{-1}. The change in $k_\perp$ results in the parabolic band becoming more intense while the flat band becomes weaker. This allows us to perform a detailed analysis of the band parameters. Fits of the ARPES maxima along the energy dispersion curves (EDCs) are indicated by the white curve in Figure 2 (c). This allows us to extract the energy of the parabolic band maximum at 0.82 eV and the effective carrier mass of $m^* \sim 0.2\ m_e$ (here m_e is the free electron mass). The position of the valence band maximum is in good agreement with STS data, which yield 0.8 eV.[?] Again, the higher (lower) ARPES intensity of the parabolic (flat) band for $k_\perp = -0.4$ Å^{-1} is nicely reproduced by our ARPES intensity calculations as can be seen in Figure 2 (d).

The distribution of photoemission intensity of GNRs in the 2D k-space is determined by the electron wave function of the particular band.[? ?] Therefore the full 2D ARPES maps are needed to unambiguously assign the experimentally observed valence bands to the calculated band structure. Figure 2 (e) depicts a constant energy slice of the ARPES map of the B-7AGNR/Au(788) system at 1.05 eV. The red arrows denote positions where the 1D parabolic band crosses the equi-energy contour. The corresponding DFT calculated map (for freestanding B-7AGNRs) is shown in Figure 2 (f), and it can be seen that the agreement is very good. Two vertical dashed lines of a blue color in Figure 2 (f) correspond to values of $k_\perp = 0$ Å^{-1} and $k_\perp = -0.4$ Å^{-1}, which we used for the ARPES momentum cuts shown in Figure 2 (a, c). Figure 2 (g) depicts experimental constant energy maps of ARPES intensity at 1.7 eV. At this energy, the weakly-dispersing band, indicated by an orange arrow in Figure 2 (g), has a maximum intensity. Similarly, the agreement to the calculated ARPES intensity, shown in Figure 2 (h) is excellent. Thus the combination of ARPES experiment and simulations allow for assignment of 1D bands of B-7AGNRs.

Let us now compare the present new results of B-7AGNR band structure to what has been reported for 7AGNRs. From our previous 2D ARPES mapping, we precisely determined the valence band structure of 7AGNRs/Au(788).[?] The VB at 0.87 eV has an effective electron

mass of $m^* \sim 0.4\ m_e$ and the VB–1 at 0.93 eV has an effective mass of $\sim 0.2\ m_e$.[?] Thus the VB–1 bands for pristine and B-doped systems have equal electron effective masses. Moreover, their energy positions are close to each other. In B-7AGNRs the VB–1 is shifted by 110 meV towards lower energy. We attribute this to the boron-mediated interaction to the Au substrate.

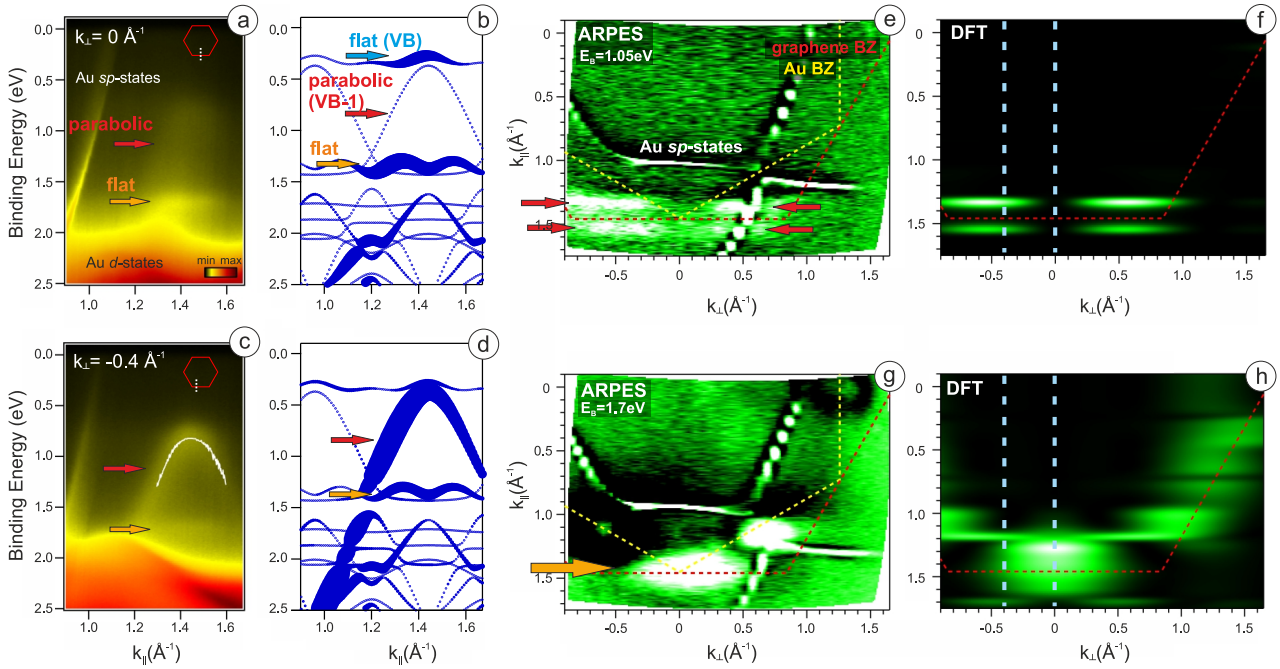

Figure 2: (a) ARPES scan of B-7AGNRs/Au(788) along $k_{\|}$ at $k_{\perp} = 0$. The red and orange arrows in the panel (a) indicate parabolic VB–1 and low energy flat band of B-7AGNRs. (b) Calculated photoemission intensity of the π-bands of freestanding B-7AGNRs for $k_{\perp} = 0$ Å^{-1}. The blue, red and orange arrows indicate the flat VB, parabolic VB–1 and lower energy band. (c) ARPES scan of B-7AGNRs/Au(788) along $k_{\|}$ at $k_{\perp} = -0.4$ Å^{-1}. The white curve in panel (c) indicates fit of the EDCs for the VB–1. (d) Calculated photoemission intensity of the π-bands of freestanding B-7AGNRs for $k_{\perp} = -0.4$Å^{-1}. (e) ARPES map at binding energy of 1.05 eV and (f) the corresponding DFT-calculated map. The red dashed line denotes the BZ edge of 2D graphene and the yellow dashed line denotes BZ edge of Au(111). Regions of high photoemission intensity coming from the parabolic band are indicated by red arrows in panel (e). (f, h) Similar as for (e, f) but at binding energy of 1.7 eV. Regions of high photoemission intensity coming from the flat band are indicated by orange arrows in panel (i). The blue vertical dashed lines in (f) and (h) indicate the direction of the ARPES cuts shown in (a, c). The experimental ARPES maps are composed of the second derivatives of the individual scans to enhance the contrast.

Electronic structure calculations

To understand interaction with the substrate better, we performed DFT calculations of the realistic B-7AGNRs/Au(111) system. To fit the periodic boundary conditions for both the ribbon and the substrate, we consider two unit cells of B-7AGNRs. The relaxed geometry is shown in Figure 3 (a) and reveals that the B atoms are attracted towards the Au substrate. Thus, the interaction between boron and the Au substrate indeed makes the ribbon structure corrugated. This is not the case for pristine 7AGNRs and explains the angular dependence of the NEXAFS intensity shown earlier. Let us now compare the calculated electronic structure of freestanding and supported B-7AGNRs, which are shown in Figure 3 (b, c). Note that doubled unit cells of B-7AGNRs/Au(111) result in the twice smaller (folded) BZ. For the freestanding system we also consider the folded band structure. This is particularly the reason why the parabolic band marked by a red arrow in Figure 3 (b) consists of two branches. The blue and the red arrows indicate two flat bands, discussed in the previous section. The contributions of B and C orbitals to π-states are denoted by red and black circles, respectively. When B-7AGNRs are adsorbed on Au(111), hybridization of the flat boron derived band (blue arrow) with Au *sp*-states affects the dispersion of this band. A part is almost degenerate with the parabolic band up to wavevector of about half the BZ length. At larger wavevectors, the band is smeared out over a large energy range. This situation renders it undetectable in ARPES measurements and probably also in STS. According to Figure 3 (c), Au-supported B-7AGNRs should have another set of weakly dispersive bands close to the Fermi level (depicted by the green arrow). This set of bands originates from the flat CB of freestanding B-7AGNRs at an energy of $\sim$0.5 eV *above* the chemical potential (see Figure 3 (b)). Our analysis of the bonding between B-7AGNR and the Au(111), shown in Supplementery Information (Fig. S3), indicates charge density accumulation in the p_z atomic-like orbitals of the B atoms that occurs with a charge density depletion in the d_z atomic-like orbitals of the Au atoms around the B sites. Though, the DFT does not capture the absolute value of the band gap[?] , it clearly indicates partial filling of the unoccupied CB by electrons. This is challenging to visualize the CB states in ARPES

experiment due to the spreading over the large energy range. However, we accumulated ARPES scan at $k_\perp$ (1.6 Å^{-1}) corresponding to the maximum matrix element for the CB states. This is shown in Figure 3(d). Let us now compare EDCs of this ARPES scan for k

=0 Å^{-1} and k

=XX Å^{-1}. This is shown in Figure 3(e). It can be seen that an extra ARPES intensity is observed for the k

=0 Å^{-1} scan. Figure 3(e) also depicts an EDC scan at identical wavevectors of the clean Au substrate. This scan also lacks the low intensity ARPES feature close to the Fermi level. This allows us to attribute this feature to the CB states that were found in the calculations (see Supplementary Information, Fig. S4 for calculations of the ARPES intensity of the CB and ARPES scans of clean Au substrate).

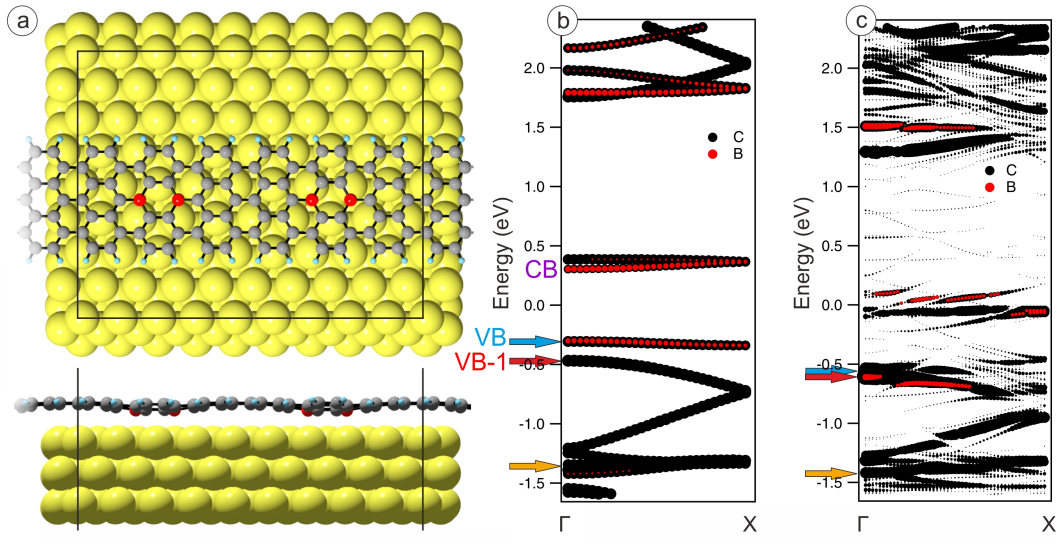

Figure 3: (a) The top and side views of the large unit cell of B-7AGNRs on Au(111), used for calculations. (b, c) Electronic band structure of freestanding B-7AGNRs and B-7AGNRs on Au(111) in folded BZ. The contributions of B and C π-bands are shown by the black and red markers, respectively. The marker size is proportional to the orbital weights, normalized per amount of atoms in the unit cell. The contribution of B states is 2 times reduced for clarity. The blue, red and orange arrows indicate the first flat valence band, the second parabolic band and the low energy flat band, correspondingly.

Our results on the energy band dispersion and orbital character of B-7AGNRs ~~can~~could also be ~~useful for analysis~~ relevant for understanding of the recent STS ~~measurements~~data

obtained from borylated segments inside 7AGNRs.[?] These experiments revealed high electron transmission for the ~~second band~~ VB–1 states and no transmission for the the ~~first band~~ frontier VB states at the junction.[?] Besides the wavefuncion symmetry arguments[?] , high transparency of the junction may be also related to~~On the basis of the present band structure this can be understood from~~ the fact that the ~~second~~ VB–1 band in B-7AGNRs has identical effective mass and is close in energy when compared to ~~the second band~~ those of 7AGNRs. The scattering associated to electron transport through the ~~first band~~ VB of 7AGNRs may be due to the strong hybridization of this band with the Au states in B-doped system.

Ultra-high vacuum Raman spectroscopy

Organoboron compounds are notoriously known for being sensitive to oxidation.[?] Indeed, we observed oxidation of B-7AGNRs after air exposure by XPS. Therefore, Raman measurements in ambient conditions are inherently unreliable. We have thus employed the UHV Raman technique,[? ?] which allows for *in situ* synthesis and Raman measurements keeping the sample always in UHV conditions. Figure 4 (a) shows a comparison of the Raman spectra of B-7AGNRs and pristine 7AGNRs on Au(111). The spectra at the bottom of Figure 4 (a) are obtained for aligned B-7AGNRs on Au(788) with laser polarization along and perpendicular to the alignment direction (that is along the Au(111) terraces). The observed anisotropy of the Raman response of aligned GNRs is a consequence of the optical selection rules and the depolarization effect.[?] The most intense feature in the presented spectra is the G-like mode (in analogy with graphene G mode) arising from the C-C bonds vibrations along the ribbon axis. Another important characteristic of the Raman spectra of GNRs is the so-called radial-breathing-like mode (RBLM). One can see that the spectral feature of aligned B-7AGNRs on Au(788) closely resemble those for non-aligned ribbons on Au(111). Small differences (for example, the maximum of the G-like peak in doped system is up-shifted by ~ 5 cm^{-1}) may be related to the inter-ribbon interaction which was also observed in the Raman spectra of densely aligned pristine 7AGNRs.[?] Since the non-interacting system is

easier, let us consider the pristine and B-doped ribbons on Au(111). We can immediately see that the Raman spectrum of B-7AGNRs has more peaks compared to the pristine 7AGNRs. It is a consequence of three times larger unit cell for B-7AGNRs resulting in three times more phonon branches, many of which have a finite Raman tensor.

Interestingly, the periodic incorporation of pairs of B atoms in 7AGNRs leads to a splitting of the prominent RBLM and G-like bands into two components. For the RBLM mode, shown in the inset of Figure 4 (a), we observe a splitting of the peak at 399 cm^{-1} in ~~pristine system to~~ 7AGNRs into peaks at 367 cm^{-1} and 386 cm^{-1} in B-7AGNRs. Similarly, for the G-like peak (at 1601 cm^{-1} for ~~pristine~~ 7AGNRs) we also observe a shift of the phonon energy to 1571 cm^{-1} and an additional component at higher energies (1543 cm^{-1}). Let us now discuss the origin of this peculiar shifts and splitting. First, the ARPES measurements allow us to rule out doping as an important contribution to the Raman shift. Even a degenerate doping and shifting of the valence band by more than 1 eV shifts the phonon modes in 7AGNRs by less than 10 cm^{-1}.? We thus attribute the observed frequency shift and splitting of the phonon modes to the lattice constant changes due to the presence of boron.

The calculations support these experimental observations. Figure 5 (b) shows the eigenvectors for RBLM and G-like phonon modes in B-7AGNRs. It can be seen that the boron atoms break vibrational degeneracy for atomic displacements in constituent sub-units with and without boron. These two sub-units are the anthracene unit containing only carbon and hydrogen and the diboroanthracene with two borons. If the atomic displacements have large amplitude in the anthracene unit, they have a low amplitude in the diboraanthracene unit and vice versa. Let us now look to the frequencies of the vibrational modes for RBLM and G-like phonons in these two structural units. The calculated frequencies for the split RBLM and G-like peaks in B-7AGNRs are also depicted in Figure 4 (b). For the RBLM we get 355 cm^{-1} and 393 cm^{-1} and for the G-like peak we find 1541 cm^{-1} and 1561 cm^{-1}. Both theoretical results are in ~~excellent~~reasonable agreement to the experimentally observed Raman frequencies. Thus the observed frequency splitting is linked to vibrations in anthracene

and diboroanthracene units which have different force constants. This nicely explains why we see a single peak in the pristine 7AGNRs. In the supplementary information we show further eigenvectors of Raman active modes for B-7AGNRs.

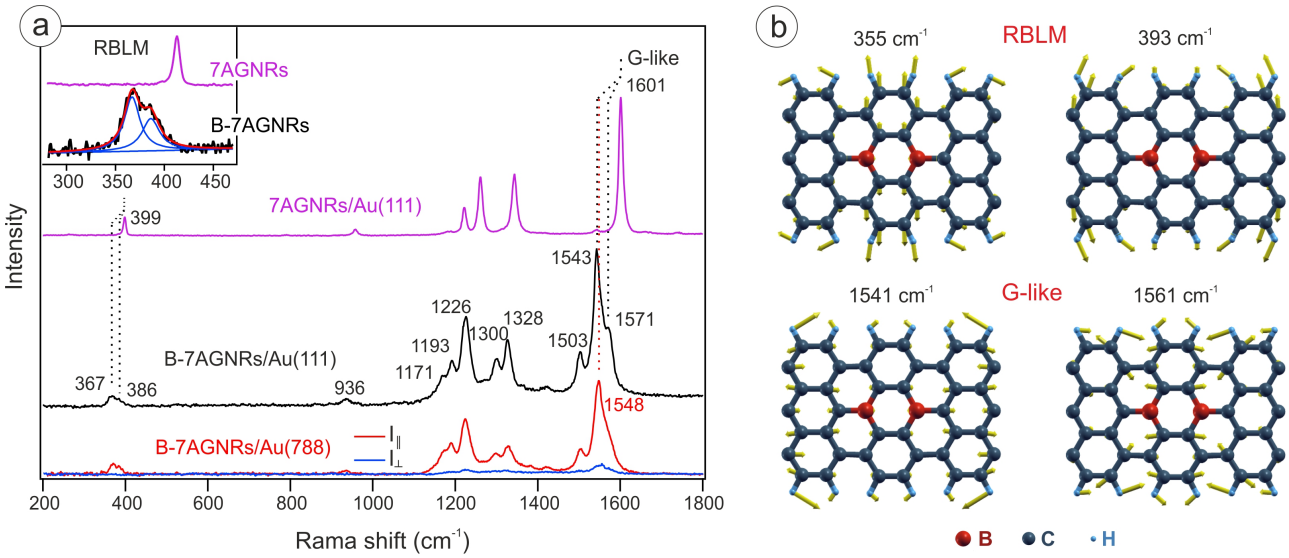

Figure 4: (a) Raman spectra of B-7AGNRs on Au(788) and on Au(111) measured by a 532 nm laser inside a UHV chamber. The spectrum of pristine 7AGNRs/Au(111) is shown at the top for comparison. Aligned B-7AGNRs/Au(788) were measured with two laser polarizations: along ($I_{\parallel}$) and perpendicular ($I_{\perp}$) to the step edges. The inset shows a zoom-in of the region of the RBLM modes for pristine 7AGNRs and boron doped B-7AGNRs. The vertical dashed lines indicate positions of RBLM and G-like Raman modes in pristine 7AGNRs and B-7AGNRs. (b) The eigenvectors of the RBLM and G-like phonon modes appearing in B-7AGNRs.

Conclusions and outlook

We have performed ~~the first full~~ a comprehensive characterization of the electronic and vibrational properties of atomically precise B-doped armchair GNRs with a width of N=7 atoms. The substitution of a pair of carbon atoms along the ribbon backbone by boron leads to profound changes in the ARPES and Raman spectra when compared to pristine 7AGNRs. Due to the charge transfer from Au to the conduction band, the B atoms are attracted to the Au substrate, which leads to periodic corrugation of the ribbon structure. Hybridization between Au and the B ~~derived~~ electronic states of the ~~first~~ valence and conduction bands (VB

and CB) causes th~~is~~ese bands to spread over a large energy region making ~~it impossible~~ them dificult to detect by ARPES and probably by STS[?] . ~~This flat band~~ requires freestanding or weakly interacting B-7AGNRs. This might be realized by decoupling B-7AGNRs from Au e.g. by intercalation of semiconductors underneath the nanoribbons.[?] As it is expected that ~~this~~ flat bands lead~~s~~ to a singularity in the density of states, it might be interesting to move the chemical potential in the vicinity of the ~~flat band~~CB and VB. We also found that the ~~second band~~ VB–1 of 7AGNRs does not change its effective mass and only weakly changes energy if boron substitution is performed. This ~~explains~~ may be relevant to the transparency of the junctions between pristine and B-doped 7AGNRs for electrons of this band. Let us discuss the impact of the current findings on the fabrication of contacts between metals and GNRs. B-GNRs likely form ideal, low-resistance Ohmic contacts to Au because their band structures are hybridized. Having a nanoribbon lying perpendicularly on a lateral Au-semiconductor interface could be means to efficiently inject carriers from Au into the nanoribbon. Finally we have overcome the limitations of traditional vibrational spectroscopy in air which is unsuitable for the investigation of B-doped 7AGNRs and found that the changes in the force constants in the vicinity of B atoms are sufficiently large to substantially modify the Raman spectra. Particularly, we observe the appearance of new characteristic phonon modes and the splitting of RBLM and G-like modes. These results demonstrate that UHV Raman spectroscopy is becoming a powerful tool for the characterization of atomically precisely functionalized GNRs which require inert conditions.

Methods

Synthesis

A monolayer of 9,10-bis(10-bromoanthracen-9-yl)-9,10-dihydro-9,10-diboraanthracene was evaporated onto a clean Au(788) surface from a Knudsen cell. The thickness of deposited organics was calibrated by quartz microbalance and XPS measurements. Hereafter the sample

was annealed in order to induce polymerization of the precursor molecule and dehydrogenation in order to form the ribbon.[??] It is known that the vicinal crystal Au(788) provides alignment of 7AGNRs along the narrow terraces with (111) surface.[?] Here we used the same approach to align B-7AGNRs.

XPS and NEXAFS

The presented XPS and NEXAFS data were obtained at the German-Russian beamline (RGBL) of the HZB BESSY II synchrotron radiation facility (Berlin, Germany). Preliminary NEXAFS experiments were also performed at the HE-SGM beamline at BESSY II. XPS spectra were measured with photon energy of 330 eV and pass energy of 5 eV in the normal emission geometry. Samples were synthesized in the UHV Raman system and transferred to the synchrotron in UHV suitcase. XPS data indicated no trace of oxygen as confirmed by the absence of an O1s peak in the scan with 700 eV photon energy. All XPS spectra were calibrated using Au $4f7/2$ core level at binding energy 84.0 eV. NEXAFS data were obtained in total electron yield (TEY) mode with energy resolution of 50 meV close to the C K-edge.

ARPES

ARPES measurements shown in this work were carried out on samples of B-7AGNRs/Au(788) synthesized *in situ* at the UE112-PGM2 beamline of HZB BESSY II with the 1^2-ARPES endstation. Preliminary ARPES data taken on samples transferred in a UHV suitcase were obtained at the ANTARES beamline of SOLEIL synchrotron[?] and at the I05 beamline of Diamond synchrotron.[?] The presented ARPES spectra were measured using a Scienta R8000 analyzer with a vertical slit and a photon energy of 45 eV and horizontally polarized light. The measurements are performed at room temperature. The experimental geometry in the ARPES experiment is determined by 3 rotational angles (polar, azimuthal and tilt angles). We align the nanoribbon sample in normal emission geometry with the direction

of 1D cutting lines (yie determine the allowed momentum in zone-folding scheme) parallel to the entrance slit of the analyzer. We then can modify the photoemission matrix element by rotating the angle corresponding to changes in $k_{\perp}$. For a horizontal slit used in our experiment this direction corresponds to the polar angle.

UHV Raman

UHV Raman measurements were performed in the back-scattering geometry using commercial Raman systems (Renishaw) integrated in a homebuilt optical chamber, where the exciting and Raman scattered light were coupled into the vacuum using a long-working distance microscope objective with an NA of ∼0.4. The analysis chamber of the UHV Raman is attached to another chamber where the B-7AGNRs on Au(111) and Au(788) were synthesized and Low-Energy Electron Diffraction (LEED) characterization were performed. Raman spectra were calibrated using Si peak at 520.5 cm^{-1} as well as oxygen peak at 1555 cm^{-1}. Polarized Raman measurements were also performed in-situ.

Calculations

The photoemission intensity was calculated using the dipole approximation for matrix element and the plane wave as a final state.[?] Density-functional-theory (DFT) calculations for the intensity simulation were carried out using the FPLO-14.00-48 code[?] utilizing the generalized gradient approximation (GGA)[?] to the exchange-correlation potential. The ribbons were assumed freestanding and hydrogen-terminated. A k-point grid of $12 \times 1 \times 1$ was used to sample the BZ. Atomic positions were relaxed until the forces on each atom were less than 10^{-2} eV/Å. The B-7AGNR/Au(111) system was modeled by a slab consisting of five Au atomic layers with a (4×9) in-plane surface unit cell and a vacuum region of at least 18 Å. The *ab initio* results for the system have been obtained with the help of the DFT by employing the GGA for the pseudopotentials generated with the projector augmented wave method (PAW)[?] as implemented in the VASP code.[? ? ?] For the structural relaxations of

the B-doped 7AGNR and the first Au surface layer, the Brillouin zone was sampled by the Γ-point with a threshold value for the calculated forces of 10 meV/Å obtained for a cutoff energy of 500 eV. More details about the electronic structure and the bonding mechanism of B-7AGNR on Au(111) are shown in Supplementary Information.

Gianni,

Acknowledgements

B.V.S., N.E., A.F. and A.G. acknowledge the ERC grant no. 648589 'SUPER-2D', funding from DFG projects CRC 1238 (project A1) and GR 3708/2-1. A.G. ackowledges INST 216/808-1 FUGG and support from the "Quantum Matter and Materials" (QM2) initiative. Research supported by the U.S. Department of Energy (DOE), Office of Science, Basic Energy Sciences (BES), under Award no. DE-SC0010409 (design, synthesis and characterization of molecular building blocks) and the Center for Energy Efficient Electronics Science NSF Award 0939514 (SPM imaging and spectroscopy). The research leading to these results has received funding from the European Community's Seventh Framework Programme (FP7/2007-2013) under grant agreement n.312284 (CALIPSO). The Synchrotron SOLEIL is supported by the Centre National de la Recherche Scientifique (CNRS) and the Commissariat 'a lEnergie Atomique et aux Energies Alternatives (CEA), France. We acknowledge Diamond Light Source for time on Beamline I05 under Proposal SI17064. The authors thank HZB BESSY II and the Russian-German Laboratory (RGBL) for the beamtime allocation. This work has been supported by the University of Cologne through the Institutional Strategy of the University of Cologne within the German Excellence Initiative.